Theoretical study of the hydroxylation of phenolates by the Cu_2O_2(N,N'-dimethylethylendiamine)$_2^{2+}$ complex

Mireia Güell,[a,b] Josep M. Luis,[a] Miquel Solà[a,*] and Per E. M. Siegbahn[b,*]

[a] Institut de Química Computacional, Universitat de Girona, Campus de Montilivi, E-17071 Girona, Spain.
[b] Department of Biochemistry and Biophysics, Stockholm University, SE 106 91, Stockholm, Sweden.

Abstract

Tyrosinase catalyses the *ortho*-hydroxylation of monophenol and the subsequent oxidation of the diphenolic product to the resulting quinone. In efforts to create biomimetic copper complexes that can oxidize C-H bonds, Stack and coworkers recently reported a synthetic μ-η^2:η^2-peroxodicopper(II)(DBED)$_2$ complex (DBED = N,N'-di-*tert*-butylethylendiamine), which rapidly hydroxylates phenolates. A reactive intermediate consistent with a bis-μ-oxo-dicopper(III)-phenolate complex, with the O-O bond fully cleaved, is observed experimentally. Overall, the evidence for sequential O-O bond cleavage and C-O bond formation in this synthetic complex suggests an alternative mechanism to the concerted or late stage O-O bond scission generally accepted for the phenol hydroxylation reaction performed by tyrosinase. In this work, the reaction mechanism of this peroxodicopper(II) complex has been studied with hybrid density functional methods by replacing DBED in the μ-η^2:η^2-peroxodicopper(II)(DBED)$_2$ complex by DMED ligands (DMED = N,N'-dimethylethylendiamine) to reduce the computational costs. The reaction mechanism obtained is compared with the existing proposals for the catalytic *ortho*-hydroxylation of monophenol and the subsequent oxidation of the diphenolic product to the resulting quinone with the aim of gaining some understanding about the copper-promoted oxidation processes mediated by 2:1 Cu(I)O_2-derived species.

Keywords

Tyrosinase, copper enzymes, biomimetic metal complexes, O_2-cleavage, density functional theory (DFT), B3LYP functional.

Introduccion

Proteins containing copper ions at their active site are usually involved as redox catalysts in a wide range of biological processes. Type-3 active site copper-containing proteins have a dicopper core, in which both copper ions are surrounded by three nitrogen donor atoms from histidine residues.[1, 2] They are able to reversibly bind dioxygen at ambient conditions. The copper(II) ions in the oxy state of these proteins are strongly antiferromagnetically coupled, leading to an EPR silent behavior. This class of enzymes is represented by three proteins, namely hemocyanin, catechol oxidase, and tyrosinase.

Tyrosinase is found in vegetables, fruits, and mushrooms, where it is a key enzyme in the browning that occurs upon bruising or long term storage. In mammals, the enzyme is responsible for skin pigmentation abnormalities, such as flecks and defects.[3] Recently, the enzyme was reported to be linked to Parkinson disease and other neurodegenerative diseases.[4, 5] Thus, tyrosinase is quite significant in the fields of medicine, agriculture, and industry.[6, 7]

Tyrosinase catalyses the *ortho*-hydroxylation of monophenol and the subsequent oxidation of the diphenolic product to the resulting quinone (Scheme 1). Little is known about the mechanistic details of the monooxygenase (phenolase) activity of tyrosinase. The enzymatic reaction is very complicated involving many fundamental catalytic processes and it is blinded by significant side reactions such as nonenzymatic transformations of *o*-quinone products to melanin pigments.[8] At least three different mechanisms for the oxidation of phenols to *o*-quinones have been suggested.

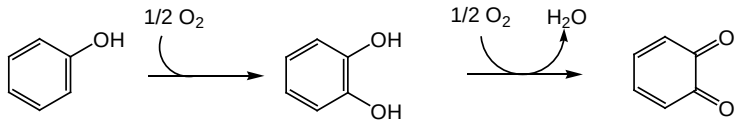

Scheme 1: Mechanism of the oxygenation and oxidation catalyzed by tyrosinase.

First, in the mechanism proposed by Solomon and coworkers in 1985,[9] the monophenol binds to the axial position of one of the coppers of the oxy site (see

Scheme 2). Then it undergoes a trigonal bipyramidal rearrangement towards the equatorial plane, which orients its *ortho*-position for hydroxylation by the peroxide. This generates a coordinated *o*-diphenolate, which is oxidized to the quinone, resulting in a deoxy site ready for further dioxygen binding.

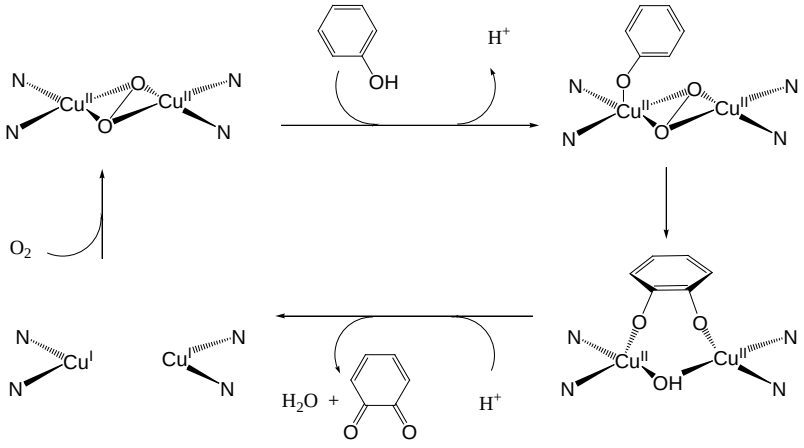

Scheme 2: Catalytic cycle for the monooxygenation of monophenols to *o*-quinones by tyrosinase suggested by Solomon and coworkers.[9]

Second, another mechanism for the oxidation of phenols to *o*-quinones catalyzed by tyrosinase was suggested from calculations using the hybrid density functional theory (DFT) B3LYP method.[10] In the proposed mechanism (see Scheme 3), the bridging hydroxide abstracts a proton from the tyrosine substrate. Then dioxygen replaces the bridging water. Subsequently, the dioxygen attacks the phenolate ring which is followed by the O-O bond cleavage. In the end, the bridging oxygen abstracts a proton from the substrate, the quinone is formed and the catalytic cycle can start again.

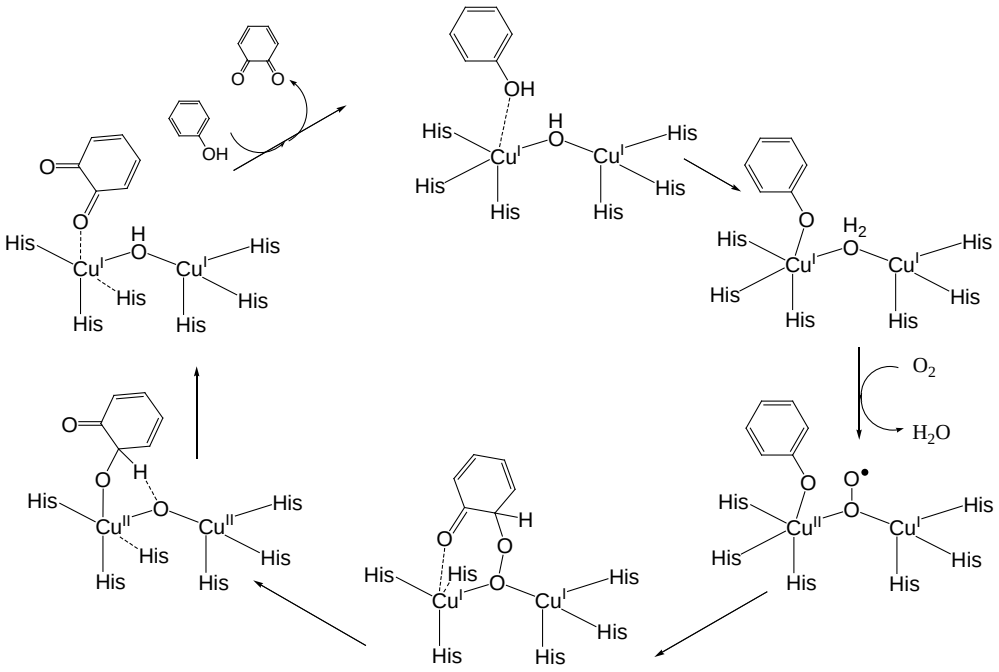

Scheme 3: Catalytic cycle of tyrosinase suggested based on hybrid DFT calculations.[10]

Finally, based on the crystal structure of tyrosinase,[11] another mechanism was suggested (Scheme 4). In this mechanism, a peroxide ion, which forms a bridge with two Cu(II) ions in the oxy form of tyrosinase, acts as a catalytic base. As a result, a proton is abstracted by the peroxide from the phenolic hydroxyl. Subsequently, the deprotonated oxygen atom of monophenol binds to Cu_B at the sixth coordination site. At this stage, Cu_B is hexacoordinated in a tetragonal bipyramidal cage. One of the two peroxide oxygens is then added to the *ortho*-carbon of monophenol. This monooxygenase reaction should be accelerated by the formation of a stable intermediate, in which the newly generated oxygen atom of diphenol binds to Cu_A. To form this state, His54, which is an axial ligand to Cu_A, must be released from the current position. This assumption is derived from the flexible feature of the residue His54 in the copper-free and Cu(II)-bound oxy forms. Simultaneously, His54 can act as a catalytic base for the deprotonation from the substrate. The resulting intermediate should easily be able to transfer two electrons to copper, resulting in the formation of the deoxy form of tyrosinase and quinone.

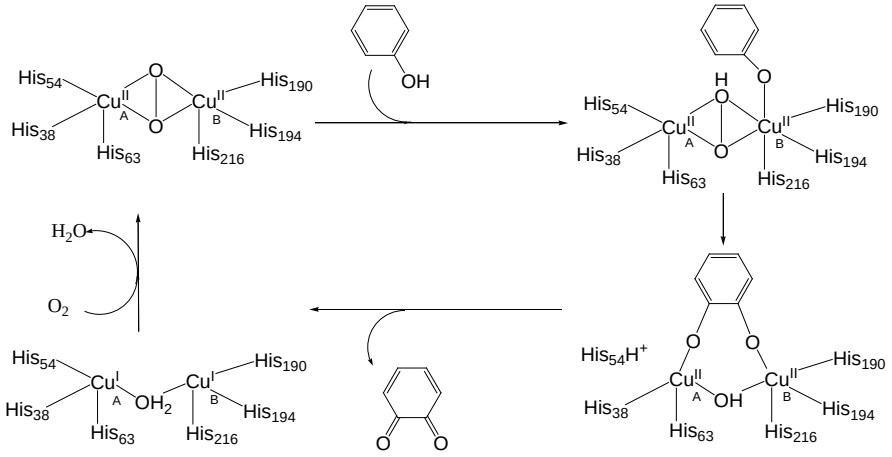

Scheme 4: Structure-based catalytic mechanism of tyrosinase suggested by Matoba et al.[11]

The order in which the O-O bond cleavage and the attack on the ring take place is not specified in the first and the third proposals described for the mechanism of tyrosinase. It is well-known that the side-on μ-η^2:η^2-peroxo species that appears in these mechanisms has an unusual electronic structure which activates it for the hydroxylation reaction.[1] The peroxide moiety is more electrophilic than in end-on peroxycopper(II) complex because of its strong σ donation to the copper ions.[12-14] Moreover, the peroxide σ^* orbital participates in the back-donation from the copper ions and consequently it weakens the O-O bond.[12-14] Besides, coordination of the monophenolic substrate would donate additional electron density into this electrophilic center and foster the hydroxylation reaction. In oxytyrosinase, the O-O bond in the oxygen intermediate involved in the best characterised metalloenzyme hydroxylation reactions, is still present.[15] Nevertheless, the direct coordination of the substrate to the copper in tyrosinase can perturb the peroxodicopper core bonding by donating electron density, which should facilitate O-O bond breaking, and also by transferring its acidic proton to the peroxide. In general, it remains an open question whether the O-O bond is cleaved prior to, concerted with, or after the attack on the ring that leads to the formation of a new C-O bond (Scheme 5).

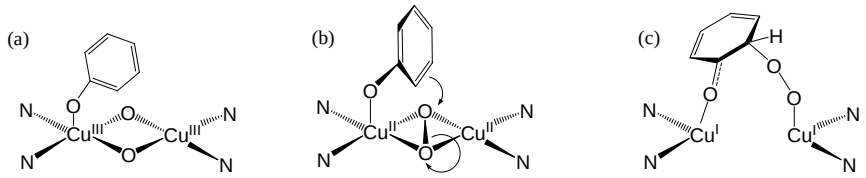

Scheme 5: Three possible mechanistic scenarios for the monooxygenation of phenol by oxytyrosinase. (a) The O-O bond cleaves prior to the attack on the ring, yielding a species which is the formally binuclear Cu(III) bis-μ-oxo complex; (b) O-O bond cleavage is concerted with the attack on the ring; (c) the O-O bond is still present after attack on the ring, yielding an aryl peroxide intermediate.[1]

The high efficiency of tyrosinase in the usually difficult C-H oxidation has elicited extensive synthetic efforts to create copper complexes that can oxidize C-H bonds.[16-25] Karlin and coworkers studied copper binuclear complexes[26-29] that showed C-H aromatic bond activation chemistry, similar to monooxygenase action. Using phenolates as substrates, a number of other research groups have described a variety of interesting and important monophenolase activity model studies.[16, 30, 31] These studies have either involved μ-η^2:η^2-peroxodicopper(II) or bis-μ-oxodicopper(III) complex reactions, leading to catechol or quinone products. Since it has been shown that the interconversion is rapid,[16, 32, 33] it is difficult to know which isomeric form is the active species in *o*-phenol hydroxylation.

Recently, Stack and coworkers reported a synthetic μ-η^2:η^2-peroxodicopper(II) complex, with an absorption spectrum similar to that of the enzymatic active oxidant, which rapidly hydroxylates phenolates at –80ºC.[31] Upon phenolate addition at extremely low temperature in solution (–120ºC), a reactive intermediate **A** consistent with a bis-μ-oxodicopper(III)-phenolate complex, with the O-O bond fully cleaved, was observed experimentally (see Scheme 6). The subsequent hydroxylation step had the hallmarks of an electrophilic aromatic substitution mechanism, similar to tyrosinase. Overall, the evidence for sequential O-O bond cleavage and C-O bond formation in this synthetic complex suggests an alternative mechanism to the concerted or late stage O-O bond scission generally accepted for the phenol hydroxylation reaction performed by tyrosinase.

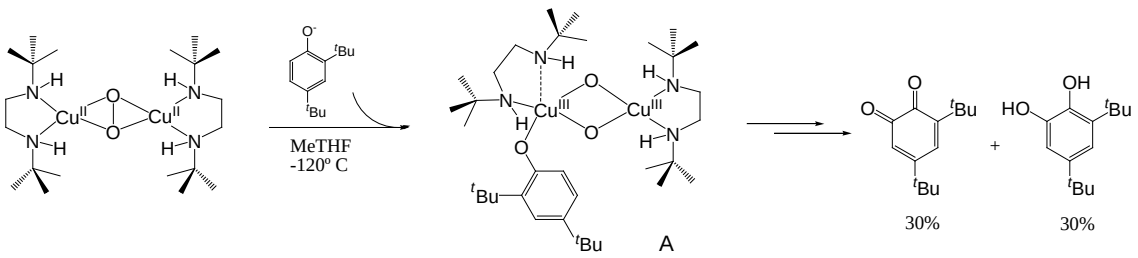

Scheme 6: Experimental results obtained by Stack and coworkers.[31]

In this work, hybrid DFT calculations have been carried out to investigate the reaction mechanism for a model of the peroxodicopper(II) complex synthesized by Stack and coworkers[31], in which the *tert*-butyl groups have been replaced by methyl groups to reduce the computational cost. This model was chosen to be as energetically representative as possible of the system studied (*vide infra*). The mechanism proposed in this work is compared with the existing proposals for the catalytic mechanism of the enzyme with the aim of gaining a deeper understanding about the chemical and biological copper-promoted oxidation processes with 2:1 Cu(I)O_2-derived species.

Methodology

All the calculations were done using the B3LYP[34, 35] hybrid density functional. Open shell systems were treated using broken-symmetry unrestricted DFT. For the open-shell structures, both the open-shell singlet and the triplet states were considered. Geometry optimizations were performed using a standard valence LACVP basis set as implemented in the Jaguar 5.5 program.[36] For the first- and second-row elements, LACVP implies a 6-31G double-ξ basis set. For the copper atoms, LACVP uses a nonrelativistic effective core potential (ECP)[37] and the valence part is described by a double-ξ basis set. Local minima were optimized using the Jaguar 5.5 program.[36] Transition states and analytical Hessians for all the stationary points (second derivatives of the energy with respect to the nuclear coordinates) were obtained using the Gaussian 03 program[38] with the same functional and basis set. The Hessians were used to determine the nature of each stationary point and to calculate zero-point energies, thermal corrections, and entropy effects. These two latter terms were computed at −120ºC. Accurate single-point energies were obtained using the cc-pVTZ(-f) basis set.[39, 40] For the copper atoms the lacv3p+ effective core potential was used. The self-consistent reaction field method implemented in Jaguar was used to

evaluate electrostatic solvation effects and compute solvent free energies.[41, 42] For the solvent methyltetrahydrofuran, MeTHF, a dielectric constant of 7.0 was used and the probe radius was set to 2.71 Å and the lacvp* basis set was used. Final free energies given in this work include energies computed at the B3LYP/cc-pVTZ(-f)&lacv3p+//B3LYP/lacvp level of theory together, with solvent effects obtained with the B3LYP/lacvp* method and with zero-point energies and thermal and entropy corrections calculated with the B3LYP/lacvp method at −120ºC.

In the literature there are several benchmark tests on the accuracy of the B3LYP functional.[43] On the basis of these results, an average error of 3-5 kcal/mol is expected for the computed relative energies for transition-metal-containing systems.[44] There are indications that the reparametrized B3LYP* functional, which uses 15% of exact Hartree-Fock (HF) exchange as compared to the 20% used in the original functional, gives a better description of the relative energies in transition-metal-containing systems.[45, 46] Therefore, the B3LYP* functional has been used to check all of the relative energies discussed below.

To study in detail the mechanism of the hydroxylation of an aromatic ring mediated by the peroxodicopper complex reported by Stack and coworkers,[31] we created a simplified model of the system. In particular, the *tert*-butyl substituents of the experimental complex have been replaced by methyl groups. Consequently, the model has DMED ligands (DMED = N,N'-dimethylethylendiamine) instead of DBED (DBED = N,N'-di-*tert*-butylethylendiamine). Furthermore, the phenolate, instead of the 2,4-di-*tert*-butylphenolate used experimentally, has been used as the substrate of the reaction. Introducing these modifications, we are changing the system and we are aware that they could have some effect into the mechanism. The experimental complex (left) and the system used in the present calculations (right) are shown in Fig. 1. In the new model, the geometry of the core and the spin density values are almost identical to the ones of the complete system (Table 1). Moreover, experimentally it has been found that the peroxo form of the N,N'-di-*tert*-butyl-ethylendiamine has a Cu-Cu distance of 3.45 Å,[31] which agrees with the results obtained here. In both cases Mulliken atomic spins of +0.43 and -0.43 on the copper atoms in the most stable open-shell singlet species are consistent with a antiferromagnetically coupling of the the two Cu(II) ions.

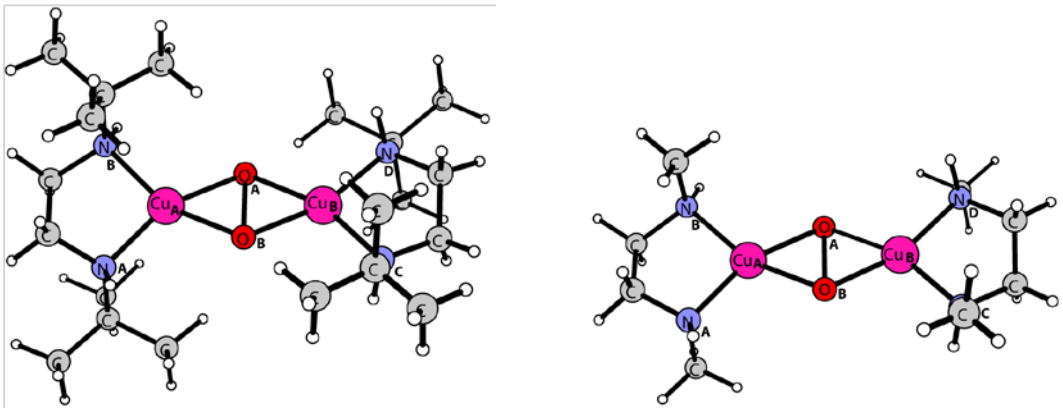

0 **1**

Fig. 1: Synthetic μ-η^2:η^2-peroxodicopper(II) complex studied by Stack and coworkers (left) and the model of the system used in this study (right).

Structures	Multiplicity[a]	Distances (Å)						Spin density			
		Cu_A-O_A	Cu_A-O_B	Cu_B-O_A	Cu_B-O_B	Cu_A-Cu_B	O_A-O_B	Cu_A	Cu_B	O_A	O_B
0	so	1.99	1.99	1.99	1.99	3.66	1.57	0.43	-0.43	0.00	0.00
	t	2.03	2.03	2.03	2.03	3.53	1.54	0.43	0.43	0.35	0.35
1	so	1.97	1.97	1.97	1.97	3.61	1.58	0.43	-0.43	0.00	0.00
	t	2.02	2.02	2.02	2.02	3.52	1.55	0.43	0.43	0.36	0.36

[a] so refers to the open-shell singlet state and t refers to triplet state.

Table 1: Comparison of geometrical parameters and spin density populations for the peroxide synthetic μ-η^2:η^2-peroxodicopper(II) complex studied by Stack and coworkers (left) and the model of this system used in the present study.

When systems with a $Cu_2O_2^{2+}$ core are studied, it is important to determine correctly the most stable coordination mode of O_2 to the two copper atoms.[47-53] This is usually a difficult task for DFT methods.[54] Experimentally, it was reported that the $Cu_2O_2(DBED)_2^{2+}$ complex consists of 95% side-on and 5% bis-μ-oxo before the interaction with the phenolate.[31, 55, 56] When using the B3LYP method with the present model, the energy difference between the peroxo and the bis-μ-oxo form is only 2.5 kcal/mol, the bis-μ-oxo being slightly more stable. Although the B3LYP theoretical study of our model complex does not give the μ-η^2:η^2-peroxodicopper(II) form as the most stable complex, the small energy difference found between the two species indicates that the two species are almost isoenergetic in line with experimental results.

To explore the effect of increasing the degree of HF exchange in hybrid methods, we have calculated the optimized geometries of the peroxo and bis-μ-oxo structures for the studied system by varying monotonically the proportion of exact exchange introduced in B3LYP-like functionals.

The nonlocal hybrid Becke's three parameter exchange functional (B3)[34] used in B3LYP was originally formulated as:

$$E_{XC} = E_X^{LSDA} + a_0\left(E_X^{exact} - E_X^{LSDA}\right) + a_x \Delta E_X^{B88} + a_c \Delta E_c^{PW91} \qquad (1)$$

The E_X^{exact}, E_X^{LSDA}, ΔE_X^{B88}, and ΔE_C^{PW91} terms are the HF exchange energy based on Kohn-Sham orbitals, the uniform electron gas exchange-correlation energy, Becke's 1988 gradient correction for exchange,[57] and the 1991 Perdew and Wang gradient correction to correlation,[58, 59] respectively. The coefficients a_o, a_x, and a_c were determined by Becke[34] by a linear least-squares fit to 56 experimental atomization energies, 42 ionization potentials, and 8 proton affinities. The values thus obtained were a_o = 0.20, a_x = 0.72, and a_c = 0.81. In the Gaussian 03[38] implementation, the expression of the B3LYP functional is similar to eq. (2) with some minor differences:[60]

$$E_{XC} = E_X^{LSDA} + a_0\left(E_X^{exact} - E_X^{LSDA}\right) + a_x \Delta E_X^{B88} + E_C^{VWN} + a_c\left(\Delta E_C^{LYP} - E_C^{VWN}\right) \qquad (2)$$

In this equation, the Perdew and Wang correlation functional originally used by Becke is replaced by the Lee-Yang-Parr (LYP)[35] one. Since the LYP functional already contains a local part and a gradient correction, one has to remove the local part to obtain a coherent implementation. This can be done in an approximate way by subtracting E_C^{VWN} from ΔE_C^{LYP}. Note that in the Gaussian 03 implementation the VWN functional is the one derived by Vosko et al. from a fit to the random phase approximation [61, 62] results.

Results and Discussion

Some authors claim that comparisons of bis-μ-oxo to side-on peroxo energies should be made with pure functionals containing no HF exchange.[48, 63] In order to study the dependence of the energy difference between the (μ-η^2:η^2)peroxodiccoper(II) and the bis-μ-oxo forms on the degree of HF exchange of the functional, we have used the Gaussian 03 program feature that allows one to vary the B3LYP standard Becke parameter set (PS) through internal options. We have changed the a_o parameter by 0.100 increments in the interval $0.000 \leq a_o \leq 0.5$, with fixed $a_x = 1 - a_o$ and $a_c = a_x$. The $a_x = 1 - a_o$ relationship has already been used in some hybrid functionals.[64, 65] In Table 2, we show the different PSs $\{a_o, a_x, a_c\}$ employed and the difference in free energy between the peroxo and the bis-μ–oxo isomers.

Parameter set	a_0	a_x	a_c	ΔG
Set 0[a]	0.000	1.000	1.000	17.6
Set 1	0.100	0.900	0.900	9.1
Set 2	0.200	0.800	0.800	-0.2
Set 3	0.300	0.700	0.700	-12.0
Set 4	0.400	0.600	0.600	-23.6
Set 5	0.500	0.500	0.500	-26.8

[a] This parameter set corresponds to the BLYP functional.

Table 2. Parameter Sets Employed for B3LYP Calculations and the corresponding relative free energies (in kcal/mol) of the peroxo form as compared to the bis-μ-oxo isomer in the $Cu_2O_2(DMED)_2^{2+}$ complex.

From the free energies of optimized isomers with the different PSs shown in Table 2, we can see that, in our $Cu_2O_2(DMED)_2^{2+}$ complex, when pure functional BLYP is used (PS 0, in Table 2), the bis-μ-oxo isomer is 17.6 kcal/mol more stable than the peroxo isomer. The more the degree of HF exchange, the more stable the peroxo form of the studied complex is. This is in line with the previous results by Cramer and coworkers.[54] It should be remarked that PS 2, whose parameters are the most similar to those used in B3LYP, is the one that best reproduces the experimental results for the $Cu_2O_2(DBED)_2^{+2}$ species showing that the energy difference between the two isomers is small. In a previous study,[55] it was shown that geometry optimizations of the peroxo species computed with the HF method and pure DFT methods either gave unreasonable geometrical parameters or converged to the bis-μ-oxo isomer. On the other hand, hybrid

DFT methods reproduced nicely the measured geometrical parameters. Consequently, we consider that B3LYP is a suitable method to carry out the study of the mechanism with our model.

The present study of the reaction mechanism of our model for the $Cu_2O_2(DBED)_2^{2+}$ complex starts from the open-shell singlet peroxo form, which is the predominant one experimentally found.[31] From this point on, two different pathways are possible. In the first one (1→ 2 → 3), the O-O bond cleavage is prior to the binding of the substrate with the complex. In the second one (1→ 2' → 3), the O-O bond cleavage takes place after the interaction of the substrate with the complex (Scheme 7).

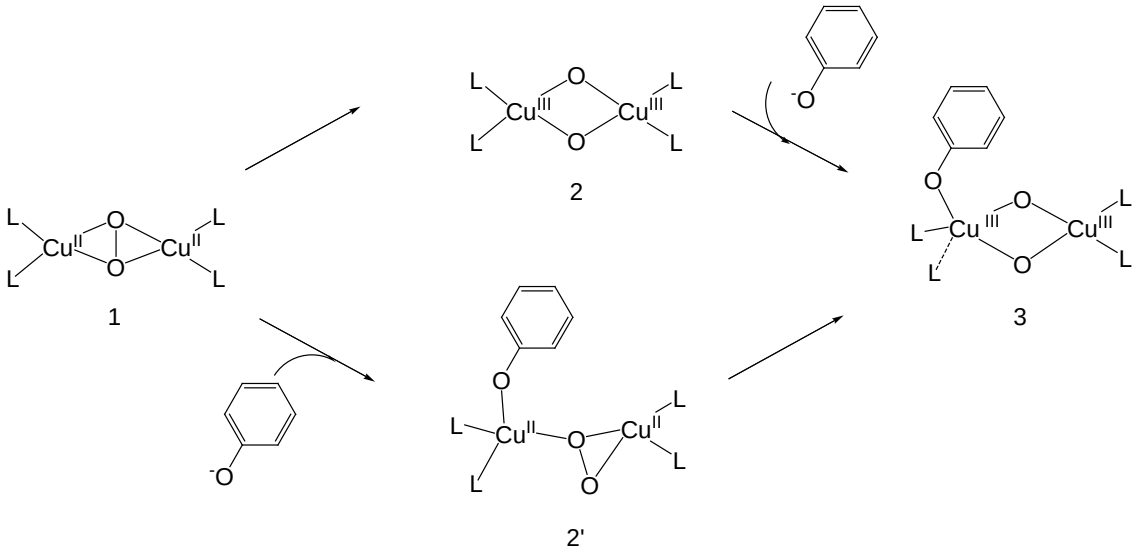

Scheme 7: Two possible ways in which the O-O can be cleaved in the studied system, before and after the binding with the substrate.

Our results for the 1→ 2 → 3 pathway showed that the barrier for the O-O bond cleavage before the phenolate is bound (TS12) is 9.6 kcal/mol. The low energy barrier of 9.6 kcal/mol found for the interconversion between the peroxo and bis-μ-oxo forms in our model systems indicate that, at this temperature, the two isomers are in equilibrium, and, therefore, the transformation of the peroxo to the bis-μ-oxo form is possible (a half-lifetime of 11.2 s is obtained for the 1→ 2 conversion in our $Cu_2O_2(DMED)_2^{2+}$ peroxo model form using the expressions derived from transition state theory[66]). At this point, it should be mentioned that the theoretical barrier for the

interconversion between the peroxo and bis-μ-oxo forms in the whole complex, i.e. $Cu_2O_2(DBED)_2^{2+}$, was found to be around 10 kcal/mol, which agrees with the value obtained for our model.[55] It is worth here to note that the calculations by Mirica and coworkers have some limitations since they were carried out only for the lowest spin state energy, without including the solvent effects, and with a partial optimization of the transition state (instead the authors took the point of maximum energy along a linear transit that transforms 1 into 2). The next stage of the reaction is the binding of the phenolate with the complex that would lead from Structure 2 to Structure 3. This step was found to be exothermic by around 16 kcal/mol (see Table 2). It should be emphasized that, for the $Cu_2O_2(DBED)_2^{2+}$ complex, the experimental energy difference between the peroxo and bis-μ-oxo isomers with sterically demanding neutral ligands is small[16, 32, 67-69], slightly favoring the peroxo form. In fact, in their work at −120ºC Stack and coworkers [31] detected that the dicopper(II) complex was 95% in the peroxo isomer (species **0** in Fig. 1) and 5% in the bis-μ-oxo.[55, 56]

On the second possible pathway (1→ 2' → 3), the free energy of binding of the substrate to the peroxo form (Structure 1) of the complex is exothermic by 31.4 kcal/mol. The next step would be the O-O bond cleavage with the substrate bound to the biomimetic complex (TS2'3) which has a barrier of more than 20 kcal/mol. This barrier is quite high since two bonds are simultaneously weakened. The O-O bond cleaves assisted basically by a single copper atom and, at the same time, the distance between the copper with the substrate bound and one of the N atoms of the ligand (Cu_A-N_B) increases considerably (Table 3).

Structures	Multiplicity[a]	Spin density					ΔG
		Cu_A	Cu_B	O_A	O_B	substrate	
1+ PhO^-	so	0.43	-0.43	0.00	0.00	-	0.0
	t	0.43	0.43	0.36	0.36	-	1.9
TS12 + PhO^- [b]	so	0.28	-0.28	0.00	0.00	-	9.6
2+ PhO^- [b]	s	-	-	-	-	-	-2.5
2'	so	0.50	-0.39	-0.07	-0.27	0.04	-31.4
	t	0.38	0.49	0.36	0.31	0.04	-31.2
TS2'3[b]	so	0.40	-0.37	-0.08	-0.05	-0.11	-9.2
3[b]	s	-	-	-	-	-	-18.8

[a] so refers to the open-shell singlet state, s refers to the closed-shell singlet state and t refers to triplet state.
[b] Only the singlet is reported, since the triplet for these structures lies much higher in energy.

Table 2: Spin density at different spin states for the structures that intervene in the core isomerisation of the Cu_2O_2 for model of the complex before (1, TS12, 2) and after (2', TS2'3, 3) the addition of the substrate. Calculated Free Energies(G), relative to Structure 1 plus phenolate, in kcal/mol are also reported.

Structures	Distances (Å)									
	Cu_A-O_A	Cu_A-O_B	Cu_B-O_A	Cu_B-O_B	Cu_A-Cu_B	O_A-O_B	Cu_A-N_A	Cu_A-N_B	Cu_B-N_C	C_B-N_D
TS12	1.87	1.87	1.87	1.87	3.16	2.01	2.00	2.00	2.00	2.00
TS2'3	1.91	1.98	1.89	1.90	3.34	1.88	2.06	2.30	2.06	2.06

Table 3: Comparison of geometrical parameters for the transition states of the O-O bond cleavage, TS12 and TS2'3.

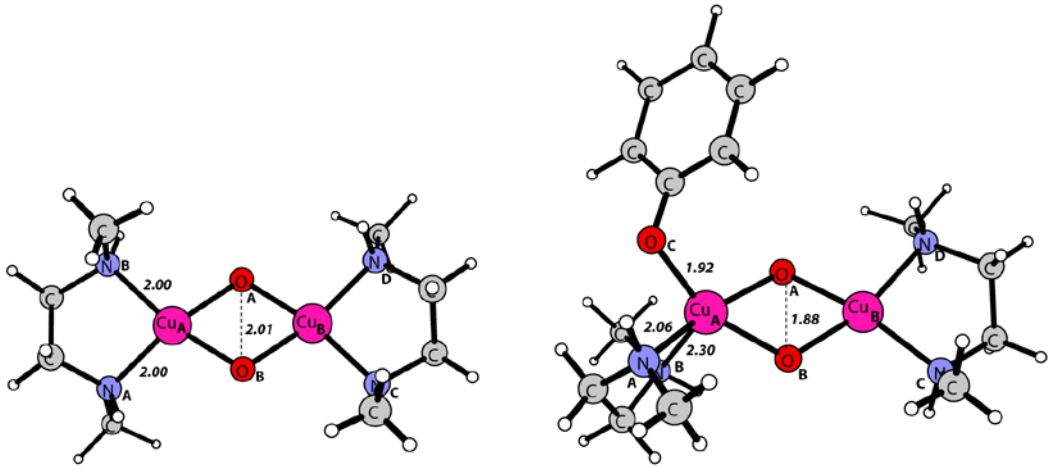

Fig. 2 Fully optimized transition states for the O-O bond cleavage TS12 and TS2'3. Distances are in angstroms.

As said before, the low energy barrier for the interconversion between the μ-η^2:η^2-peroxodicopper(II) and the bis-μ-oxodicopper(II) isomers suggests that these two

forms are in equilibrium at −120 ºC. Although our theoretical calculated energies favour slightly the bis-μ-oxo form, the experimental results for species **0** in Fig. 1 indicate that this equilibrium is displaced towards the peroxo isomer. [31, 55, 56] The added phenolate can react with any of the two forms since reaction of phenolate with the peroxo and bis-μ-oxo isomers are exothermic processes with reaction free energies of −30.8 and −16.3 kcal/mol, respectively. In absence of any other kinetic constraint, the added phenolate will react with the peroxo form according to the experimental observation of this species in solution[31] or with the bis-μ-oxo isomer as indicated by our calculations. It is worth mentioning that, for the addition of fragments of different charge (such as addition of phenolate to species 1 or 2), solvent effects are extremely important and difficult to handle correctly. For this reason, we consider that to definitely differentiate between routes 1→ 2 → 3 and 1→ 2' → 3 further calculations including explicitly solvent molecules in the model are necessary. In addition, a study of the reaction dynamics might be necessary to reach a final answer about this initial part of the reaction mechanism. At the present stage, solvent effects have been introduced using an approximate polarizable continuum model. The approximate nature of such calculations prevents us to definitely reject any of the two pathways proposed.

Experimentally, an intermediate where the distance between the two copper ions is 2.79 Å and with an average distance of 1.89 Å between each Cu and the four N/O ligands was detected (species **A** in Scheme 6).[31] The observed structure should correspond to Structure 3 that has a distance of 2.86 Å between the copper ions and an average distance of 1.92 Å of each Cu with the four N/O ligands (Table 4). Previously, Stack and coworkers already optimized a structure that corresponds to our Structure 3 and the intermediate detected experimentally.[31] It should be mentioned that their model includes the whole complex and the 2,4-di-*tert*-butylphenolate as substrate, which is the substrate used experimentally. They used the unrestricted B3LYP hybrid functional with the 6-311G* basis set for the copper atoms and the 6-31G* basis set for each remaining atoms. Despite using different models and basis sets, the geometrical parameters they obtained are quite similar to the ones that we have found in the present study (see Table 4).

Structures	multiplicity[a]	Distances (Å)											
		Cu_A-O_A	Cu_A-O_B	Cu_B-O_A	Cu_B-O_B	Cu_A-Cu_B	O_A-O_B	Cu_A-O_C	O_A-C_A	Cu_A-N_A	Cu_A-N_B	Cu_B-N_C	Cu_B-N_D
3[b]	s	1.88	1.92	1.82	1.82	2.86	2.37	1.92	3.16	2.04	2.43	2.02	2.02
	s[c]	1.80	1.86	1.76	1.78	2.76	2.31	1.84	1.34	2.00	2.83	2.02	1.97
TS34	s	1.93	1.88	1.88	1.84	2.92	2.38	1.93	2.10	2.10	2.28	2.03	2.03
	t	1.96	1.95	1.88	1.85	2.90	2.48	2.08	2.26	2.08	2.30	2.07	2.07
4	so	2.07	1.90	2.01	1.89	2.88	2.66	2.12	1.43	2.18	2.22	2.07	2.12
	t	2.06	1.90	2.00	2.00	2.89	2.67	2.12	1.43	2.18	2.22	2.17	2.14

[a] so refers to the open-shell singlet state, s refers to the closed-shell singlet state and t refers to triplet state.
[b] Only the singlet is reported, since the triplet for this structure lies much higher in energy.
[c] Geometrical parameters corresponding to the structure equivalent to Structure 3 found previously by Stack and coworkers.[31]

Table 4: Comparison of geometrical parameters transition state for the structures that intervene in the C-O bond formation.

In Structure 3, the attack on the ring by one of the oxygen atoms takes place (Scheme 8). The formation of a new C-O bond breaks the aromaticity of the phenolate and spin density appears on both copper ions (Table 5). The transition state TS34 was located for both the closed-shell singlet and triplet cases. The singlet structure for TS34 (Fig. 3), with a barrier of 7.2 kcal/mol, is more stable than the triplet by 1 kcal/mol but the structures are almost identical. In this step the distance between Cu_A-N_B decreases from 2.43 to 2.22 Å while the distance between Cu_A-O_C increases from 1.92 to 2.12 Å. According to preliminary calculations at the B3LYP level by Stack and coworkers,[31] the activation energy for the C-O bond formation step is 10.9 kcal/mol (a value 12 kcal/mol is given in the supporting information [31]). This value corresponds to the point of maximum energy along a linear transit that transforms 3 into 4 by approaching in successive steps the *ortho*-carbon of the phenolate and the closest oxygen atom of the Cu_2O_2 core. No full optimization of the transition state was carried out in that work and, therefore, the barrier of 10.9 kcal/mol should be taken as an upper bound to the actual energy barrier.[31] Indeed, this value is higher by 4.8 kcal/mol than that obtained in the present work by fully optimizing the transition state structure. It is also worth noting that in a previous and recent B3LYP study[70] using a similar basis set on a different $Cu_2O_2(L_2)^{+2}$ model, the authors were unable to locate a TS similar to our TS34. Instead, they found an $(\mu\text{-}\eta^1\text{:}\eta^1)Cu_2(I,II)O_2$ intermediate that reacts to give the analogous of our structure 4 through a TS with an energy barrier of about 16 kcal/mol. Despite several attempts to find it, such a $(\mu\text{-}\eta^1\text{:}\eta^1)Cu_2(I,II)O_2$ intermediate has not been found in our potential energy surface.

The thermal decay rates at −105ºC for species **A** (see Scheme 6) formed with 6-d-2,4-di-*tert*-butylphenolate and 6-h-2,4-di-*tert*-butylphenolate were measured by Stack and coworkers and they obtained a KIE of 0.83±0.09.[31] Using our model and the following expression derived from the transition state theory:[66]

$$KIE = \frac{k_H}{k_D} = \frac{\frac{k_B T}{h}(c^0)^{\Delta n} e^{-\left(\Delta G_H^{\neq}/RT\right)}}{\frac{k_B T}{h}(c^0)^{\Delta n} e^{-\left(\Delta G_D^{\neq}/RT\right)}} = e^{-\left(\left(\Delta G_H^{\neq} - \Delta G_D^{\neq}\right)/RT\right)} \qquad (3)$$

we obtained a KIE of 0.88 at −105ºC, which is in excellent agreement with the reported experimental value. Such small secondary inverse kinetic isotope effect is generally anticipated for electrophilic aromatic substitution (EAS) reactions, in which a carbon centre undergoes a hybridization change from sp^2 to sp^3 in the transition state. As it can be seen in Fig. 3, this is exactly what happens in TS34. The calculated free energy barrier of 7.2 kcal/mol and the KIE of 0.88 for the transformation of 3 into 4 perfectly matches the experimental 10.3 kcal/mol and 0.83 values, thus reinforcing the idea that this step is the rate determining step for the transformation of **A** (Scheme 6) into the final products (but not for the full transformation from **0** to products!).

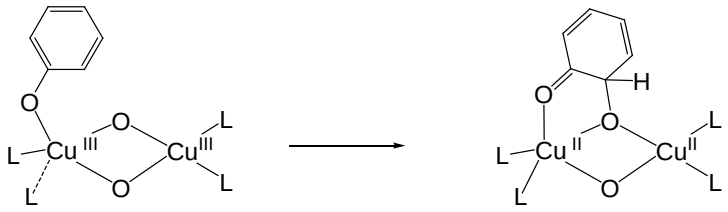

3 4

Scheme 8: C-O bond formation in the studied system.

Structures	multiplicity[a]	Spin density					ΔG
		Cu_A	Cu_B	O_A	O_B	substrate	
3[b]	s[b]	-	-	-	-	-	-18.8
TS34	s	-	-	-	-	-	-11.6
	t	0.57	0.42	0.11	-0.10	0.80	-10.6
4	so	0.55	-0.47	0.00	-0.11	0.02	-44.9
	t	0.53	0.44	0.11	0.67	0.04	-46.2

[a] so refers to the open-shell singlet state, s refers to the closed-shell singlet state and t refers to triplet state.
[b] Only the singlet is reported, since the triplet for this structures lies much higher in energy.

Table 5: Spin density at different spin states for the structures that intervene in the C-O bond formation. Calculated Free Energies(G), relative to Structure 1 plus the phenolate, in kcal/mol are also reported.

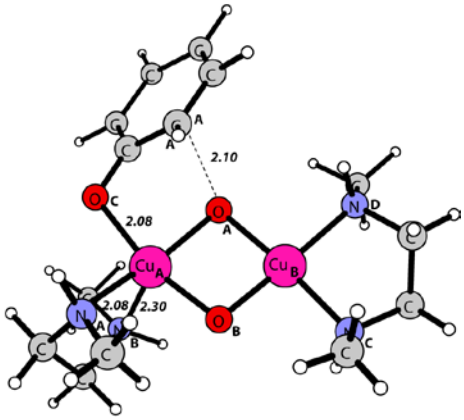

Fig. 3: Fully optimized transition state for the open-shell singlet state for the C-O formation (TS34). Distances are in angstroms.

In Structure 4 the distance between the hydrogen atom of the ring that has to be transferred and O_B is too long for the transfer to take place. For this reason there is a rearrangement of the position of the substrate that transforms 4 into 5 (Fig. 4 shows the transition state of this transformation). This reduces the O_B-H_A distance from 4.13 to 3.72 Å and increases the Cu_A-O_C distance from 2.12 to 2.40 Å. This step has a barrier of 0.3 kcal/mol with the small basis set. However, after carrying out the single-point energy calculation with the bigger basis set and adding the effect of the solvent, the thermal corrections and entropy effects, it turns out to be barrierless. It should be mentioned that for the experimentally reported $Cu_2O_2(DBED)_2^{2+}$ complex,[31] due to presence of the bulky *tert*-butyl substituents of the ligand, this step may possibly have a significant barrier since the whole system will have a larger steric hindrance for rotation.

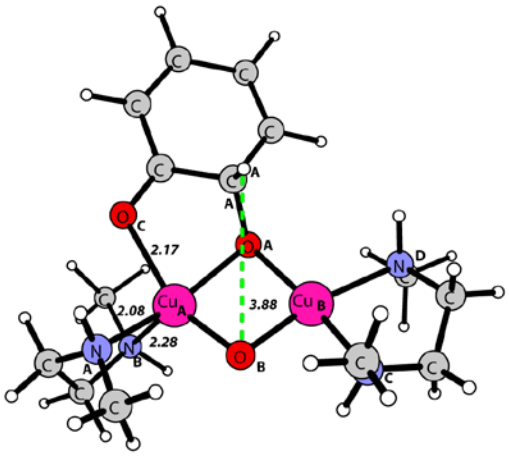

Fig. 4: Fully optimized transition state for the triplet state for rearrangement of the position of the substrate (TS45). Distances are in angstroms.

After the rearrangement of the position of the substrate, the transfer of the hydrogen can finally occur (Scheme 9). The O_B-H_A distance goes from 3.72 in Structure 5 to 0.97 Å in Structure 6. Along this process, the ring of the substrate recovers the aromaticity (Table 6 and Fig. 5). For this step, the open-shell singlet and triplet states both have a barrier of 4.7 kcal/mol (Table 6). As can be seen in Table 6, the geometrical parameters are almost identical for the two different spin states. Similar energies and geometries in the open-shell singlet and triplet states of 5 and also of TS56 are an indication that the two spins are weakly coupled for these species. Some spin density also appears on the ring after the hydrogen atom transfer (Table 7, species 6). The lack of spin density and the positive charge (0.47 e) on the H transferred in TS56 leads us to conclude that the process is a proton transfer in the transition state which is subsequently followed by an electron transfer. So, at the end, what has been transferred is a hydrogen atom, although in the TS56 the particle transferred has to be considered a proton.

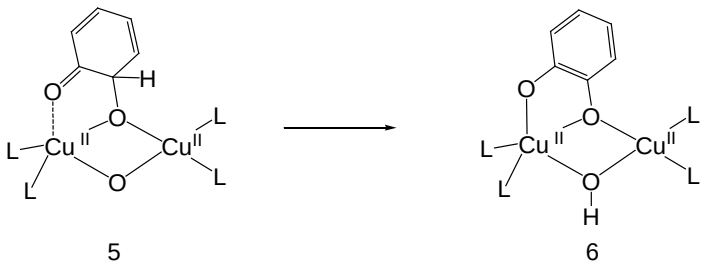

Scheme 9: Hydrogen atom transfer in the studied system.

Structures	Multiplicity[a]	Distances (Å)										
		Cu_A-O_A	Cu_A-O_B	Cu_B-O_A	Cu_B-O_B	Cu_A-Cu_B	O_A-O_B	O_A-C_A	Cu_A-N_A	Cu_A-N_B	C_A-H_A	O_B-H_A
5	so	2.09	1.89	2.03	1.87	2.89	2.66	1.43	2.09	2.14	1.12	3.72
	t	2.09	1.90	2.03	1.88	2.89	2.66	1.43	2.09	2.14	1.12	3.72
TS56	so	2.09	1.98	2.03	1.92	2.76	2.52	1.47	2.06	2.11	1.26	1.53
	t	2.09	1.98	2.04	1.93	2.76	2.51	1.47	2.06	2.11	1.26	1.52
6	so	2.03	2.02	2.04	1.94	3.00	2.61	1.38	2.06	2.23	4.77	0.97
	t	2.06	1.97	2.08	1.94	2.99	2.61	1.94	2.10	2.27	4.78	0.97

[a] so refers to the open-shell singlet state and t refers to triplet state.

Table 6: Comparison of geometrical parameters transition state for the structures that intervene in hydrogen atom transfer.

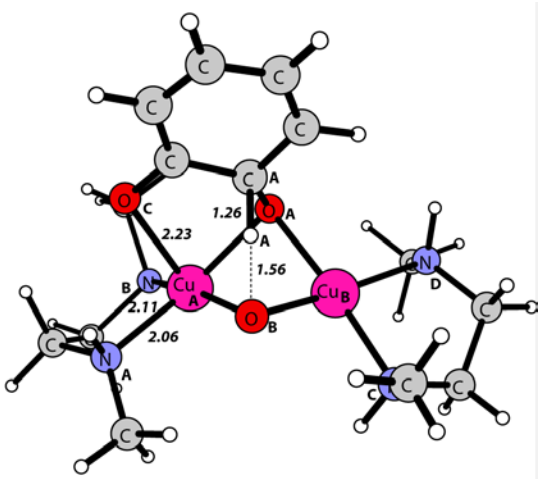

Fig. 5: Fully optimized transition state for the triplet state for the hydrogen atom transfer (TS56). Distances are in angstroms.

Structures	Multiplicity[a]	Spin denstity					ΔG
		Cu_A	Cu_B	O_A	O_B	substrate	
5	so	0.53	-0.47	-0.03	-0.03	0.01	-48.8
	t	0.50	0.44	0.15	0.65	0.01	-50.2
TS56	so	0.42	-0.53	0.04	0.08	0.01	-44.1
	t	0.50	0.40	0.30	0.52	0.00	-45.5
6	so	0.61	-0.41	-0.09	-0.02	-0.10	-93.7
	t	0.61	0.37	0.26	0.11	0.38	-94.3

[a] so refers to the open-shell singlet state and t refers to triplet state.

Table 7: Spin density at different spin states for the structures that intervene in hydrogen atom transfer. Calculated Free Energies (G), relative to Structure 1 plus the phenolate, in kcal/mol are also reported.

After the hydrogen atom transfer, the last step of the reaction should consist of the transfer of two electrons from the complex, one from each one of the copper ions, to

the substrate to complete its reduction. This step is endothermic by 9.2 kcal/mol. This means that the barrier would probably be higher in energy than all the barriers found for the previous steps of the reaction that starts from structure 3. However, it should be mentioned that experimentally an acid is added in order to obtain the products (the quinone and the catechol), so the added protons are probably necessary for the last stage of the reaction.

The free energies for the reaction mechanism studied in this work using the $Cu_2O_2(DMED)_2^{2+}$ complex are shown in Fig. 6. The reaction starts with the Cu_2-(II-II)-peroxo form of the complex in equilibrium with the Cu_2-(III-III)-bis-μ-oxo isomer and this is the situation when phenolate is added. At this stage, two scenarios are possible. Either the O-O bond cleavage takes place before the binding of the substrate, or the O-O bond cleaves after the binding of the substrate. Subsequently the attack on the ring of one of the oxygen atoms occurs. In order to make possible the hydrogen atom transfer from the ring to the second oxygen of the complex, a rearrangement of the position of the substrate takes place. Finally, the hydrogen atom is transferred from the substrate to the complex and the addition of protons would make possible the formation of the products, the quinone and the catechol, that are observed experimentally.

In both possible scenarios the most critical step is the peroxide O-O bond cleavage and this step is prior to the attack on the ring that leads to a new C-O bond formation. For the step corresponding to the hydroxylation of the ring, the calculated free energy barrier (7.2 kcal/mol) and KIE (0.88) are in good agreement with the experimental values (10.3 kcal/mol and 0.83, respectively), thus providing confidence about the validity of the obtained results.

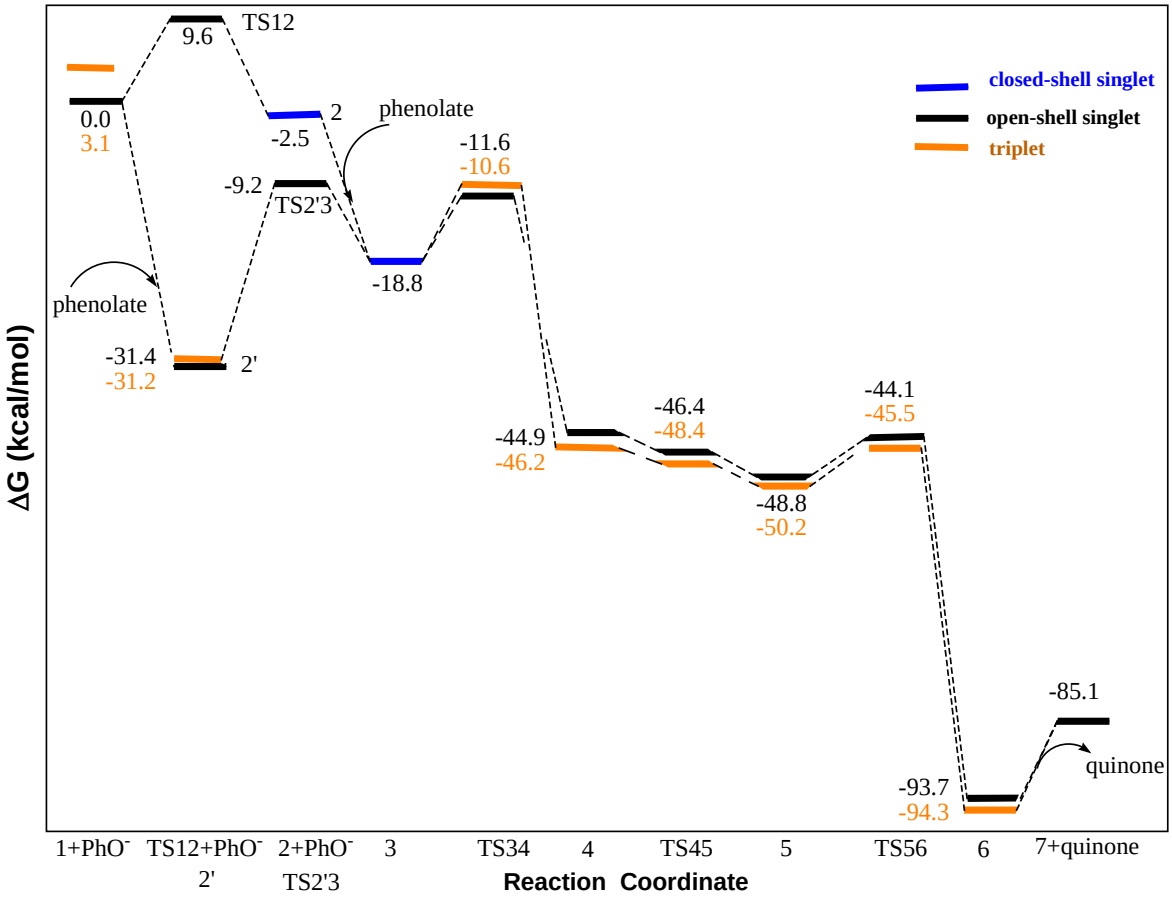

Fig. 6: Free energy profile obtained for the mechanism studied at the B3LYP level of theory. Calculated Free Energies(G), relative to structure 1 plus phenolate, are given in kcal/mol.

Finally, all the structures were also reoptimized using the B3LYP* functional, with only 15% HF exchange. As can be seen in Table 8, rather small effects were obtained from a decrease in the amount of exact exchange. The main changes occur for the relative energies of structures 2 and 3 with bis-μ-oxo character that, as discussed before (Table 2), are stabilized with the reduction of the HF exchange contribution to the hybrid density functional. For none of the intermediates or transition states, B3LYP and B3LYP* give different ground states. These results give further support to the reliability of the method used in the present work.

Structures	B3LYP		B3LYP*	
	ΔG(S=0)	ΔG(S=1)	ΔG(S=0)	ΔG(S=1)
1+ PhO^-	0.0	1.9	0.0	4.0
TS12+ PhO^-	9.6	-	7.9	-
2+ PhO^-	-2.5	-	-7.2	-
2'	-31.4	-31.2	-30.8	-30.4
TS2'3	-9.2	-	-10.6	-
3	-18.8	-	-24.1	-
TS34	-11.6	-10.6	-17.4	-11.3
4	-44.9	-46.2	-43.3	-48.9
TS45	-46.4	-48.4	-44.7	-46.6
5	-48.8	-50.2	-47.2	-52.0
TS56	-44.1	-45.5	-44.0	-45.7
6	-93.7	-94.3	-92.8	-97.4
7	-85.1	-	-82.4	-

Table 8: Calculated free energies(G) in kcal/mol for different spin states for the structures that appear in the hydroxylation of phenolate for the model of the complex.

Before comparing the results obtained for the studied synthetic complex with the existing proposals for the catalytic cycle for tyrosinase, several facts have to be taken into account. For most of the biomimetic systems of tyrosinase, including the system studied in this article, the substrate is an anion, a phenolate, while for the enzyme the substrate is neutral, a phenol. Tyrosinase is thought to be capable of abstracting the proton of the phenol that it releases later to give the products. On the other hand, for the studied complex, protons have to be added in the last step of the reaction in order to obtain the quinone and/or the catechol. Moreover, since tyrosinase biomimetic complexes cannot restart the reaction by themselves, the reaction assisted by these compounds can be more exothermic than the reaction catalyzed by the enzyme.

In the proposal made by Solomon and coworkers for the tyrosinase mechanism (Scheme 2),[9, 71, 72] in the first step the phenol loses one proton before binding to one of the copper atoms of the active site. At his point, it should be highlighted that from the spectral features of oxy-tyrosinase Solomon and coworkers proved that it has a very similar active site to oxy-hemocyanin.[71] For the tyrosinase mechanism, the O-O bond cleavage and the attack on the ring results in the formation of a coordinated *o*-diphenolate intermediate that has a simultaneous coordination of the substrate to both copper centers in a bidentate bridging fashion was suggested.[9, 72] In our proposed

mechanism for the hydroxylation of phenolates by Cu_2O_2(N,N'-dimethylethylendiamine)$_2^{2+}$ such species does not intervene. The closest structure in our mechanism to the intermediate suggested by Solomon and coworkers for the enzyme catalytic cycle is species 6 which has one of the oxygen atoms of the substrate bound to one of the copper ions and the other bound to both copper ions. For our model, we tried to locate a structure with the substrate coordinated to both copper centers in a bidentate bridging fashion as suggested by Solomon et al.[9] Nevertheless, all attempts to find such species lead to structure 6 with only one of the oxygen atoms coordinated to both copper atoms. So, at least with the present model and level of calculation, the possibility of a reaction mechanism going through the intermediate suggested by Solomon and coworkers[9] has to be rejected *in our model*. Obviously, from our calculations the presence of such an intermediate cannot be ruled out in the reaction mechanism of tyrosinase.

In the mechanism suggested by Matoba et al. (Scheme 4) for tyrosinase,[11] the proton of the phenol does not leave the active site of the enzyme until the last step of the catalytic cycle. First, it is bound to one of the oxygen atoms of the peroxide moiety and then to Histidine 54. Later it forms the water molecule that is released in the last stage. Since for the present studied complex, the reaction starts with the phenolate and the protons are introduced to obtain to products, comparisons cannot be made for this point. In Matoba's proposal,[11] the binding mode of the substrate after the O-O bond cleavage and the attack on the ring is the same suggested by Solomon. As said before, such intermediate was not found in the potential energy surface of our model.

It is also worth noting that in both Solomon and Matoba's proposals the order in which the O-O bond cleavage and the attack on the ring occur in the catalytic cycle for the phenolase activity of tyrosinase is not clearly specified and, therefore, it can not be discussed in relation to our proposal. However, in both mechanisms, the O-O bond remains after the binding of the phenolate and the coordination environment of the two copper ions with the oxygen atoms, $Cu(II)_2$-μ-η^2:η^2-O_2, is not modified and this is at variance with the reaction mechanism reported in this work. In our theoretical study for the Cu_2O_2(N,N'-dimethylethylendiamine)$_2^{2+}$ complex, when the substrate is bound to one of the copper ions there are two possible coordination environments. A structure with an asymmetric $Cu(II)_2$-μ-η^1:η^2-O_2 core is proposed if the substrate binds to one of

the copper ions previous to the O-O bond cleavage. On the other hand, a $Cu(III)_2$-(μ-O_2) structure is suggested after the O-O cleavage takes places, which corresponds to the intermediate observed experimentally by Stack and coworkers (species **A** in Scheme 6).[31]

Finally, our study for the Cu_2O_2(N,N'-dimethylethylendiamine)$_2^{2+}$ complex cannot be directly compared with the proposal made in the earlier hybrid DFT study by one of us for tyrosinase (Scheme 3) [10] for several reasons. In the first place, the total charge in the previous study was +1 while in the current model is +2. Secondly, in that study the Cu_2-(II-II)-peroxo form of the complex that we use as the starting point for our mechanism does not appear. Finally, the previous mechanism went through an intermediate with a superoxo moiety that we have been unable to locate in our potential energy surface and not via the structure 3 (intermediate **A**) that has been detected experimentally.

Conclusions

In this work, we have studied the full reaction mechanism of the hydroxylation of phenols mediated by the Cu_2O_2(N,N'-dimethylethylendiamine)$_2^{2+}$ complex. The proposed reaction mechanism follows an electrophilic aromatic substitution pattern that involves an intermediate with the O-O bond cleaved and the phenolate coordinated to a copper center. This species would correspond to the intermediate observed experimentally by Stack and coworkers.[31] The rate determining step for the hydroxylation of this intermediate to the final products is the attack of one oxygen atom of the Cu_2O_2 unit to the aromatic ring leading to a new C-O bond. The barrier and the KIE for this ring hydroxylation step obtained with the B3LYP functional are in good agreement with the experimental results.[31] After this step, in our model complex, the reaction proceeds with smooth energy barriers until the final quinone products are reached. Unfortunately, our calculations cannot definitely assign whether the O-O cleavage takes place before or after the binding of the substrate. In our opinion, to get a definitive answer on these first steps of the studied reaction mechanism, it is necessary to include explicitly several solvent molecules in the model and to perform a study of the dynamics of the reaction. This is out of the scope of the present work but it will be the subject of future research in our laboratory.

Finally, although the obtained results refer *only* to the system studied, we consider that our study may offer some hints on the reaction mechanism of tyrosinase. For this reason, the existing proposals for the tyrosinase catalytic cycle mechanism and our theoretical mechanism for Cu_2O_2(N,N'-dimethylethylendiamine)$_2^{2+}$ complex have been compared and discussed as to the similarities and differences found.

Acknowledgements

Financial help has been furnished by the Spanish Ministerio de Educación y Ciencia (MEC) projects No. CTQ2005-08797-C02-01/BQU and CTQ2008-03077/BQU and by the Catalan Departament d'Universitats, Recerca i Societat de la Informació (DURSI) of the Generalitat de Catalunya project No. 2005SGR-00238. We thank Dr. Miquel Costas for valuable discussions and the reviewers for helpful comments. M.G. thanks the Spanish MEC for a Ph.D. grant.

Supporting Information Available: Optimized cartesian xyz coordinates of all stationary points located on the PES for the reaction mechanism studied at the B3LYP/lacvp level of theory.

References

1. Solomon EI, Sundaram UM, Machonkin TE (1996) Chemical Reviews 96:2563-2605
2. Solomon EI, Baldwin MJ, Lowery MD (1992) Chemical Reviews 92:521-542
3. Oetting WS (2000) Pigment Cell Research 13:320-325
4. Xu YM, Stokes AH, Roskoski R, Vrana KE (1998) Journal of Neuroscience Research 54:691-697
5. Asanuma M, Miyazaki I, Ogawa N (2003) Neurotoxicity Research 5:165-176
6. Parvez S, Kang M, Chung HS, Bae H (2007) Phytotherapy Research 21:805-816
7. de Faria RO, Moure VR, Amazonas M, Krieger N, Mitchell DA (2007) Food Technology and Biotechnology 45:287-294
8. Sánchez-Ferrer A, Rodríguez-López JN, García-Cánovas F, García-Carmona F (1995) Biochimica Et Biophysica Acta-Protein Structure and Molecular Enzymology 1247:1-11
9. Wilcox DE, Porras AG, Hwang YT, Lerch K, Winkler ME, Solomon EI (1985) Journal of the American Chemical Society 107:4015-4027
10. Siegbahn PEM (2003) Journal of Biological Inorganic Chemistry 8:567-576
11. Matoba Y, Kumagai T, Yamamoto A, Yoshitsu H, Sugiyama M (2006) Journal of Biological Chemistry 281:8981-8990
12. Ross PK, Solomon EI (1990) Journal of the American Chemical Society 112:5871-5872
13. Ross PK, Solomon EI (1991) Journal of the American Chemical Society 113:3246-3259
14. Baldwin MJ, Root DE, Pate JE, Fujisawa K, Kitajima N, Solomon EI (1992) Journal of the American Chemical Society 114:10421-10431
15. Eickman NC, Solomon EI, Larrabee JA, Spiro TG, Lerch K (1978) Journal of the American Chemical Society 100:6529-6531
16. Lewis EA, Tolman WB (2004) Chemical Reviews 104:1047-1076
17. Hatcher LQ, Karlin KD (2004) Journal of Biological Inorganic Chemistry 9:669-683
18. Hatcher LQ, Karlin KD (2006) Advances in Inorganic Chemistry Including Bioinorganic Studies 58:131-184
19. Costas M, Ribas X, Poater A, López Balvuena JM, Xifra R, Company A, Duran M, Solà M, Llobet A, Corbella M, Usón MA, Mahía J, Solans X, Shan X, Benet-Buchholz J (2006) Inorganic Chemistry 45:3569-3581
20. Ribas X, Xifra R, Parella T, Poater A, Solà M, Llobet A (2006) Angewandte Chemie-International Edition 45:2941-2944
21. Brackman W, Havinga E (1955) Recueil Des Travaux Chimiques Des Pays-Bas-Journal of the Royal Netherlands Chemical Society 74:1021-1039
22. Brackman W, Havinga E (1955) Recueil Des Travaux Chimiques Des Pays-Bas-Journal of the Royal Netherlands Chemical Society 74:1070-1080
23. Brackman W, Havinga E (1955) Recueil Des Travaux Chimiques Des Pays-Bas-Journal of the Royal Netherlands Chemical Society 74:1100-1106
24. Brackman W, Havinga E (1955) Recueil Des Travaux Chimiques Des Pays-Bas-Journal of the Royal Netherlands Chemical Society 74:1107-1118
25. Brackman W, Havinga E (1955) Recueil Des Travaux Chimiques Des Pays-Bas-Journal of the Royal Netherlands Chemical Society 74:937-955
26. Karlin KD, Cruse RW, Gultneh Y, Hayes JC, Zubieta J (1984) Journal of the American Chemical Society 106:3372-3374

27. Nasir MS, Cohen BI, Karlin KD (1992) Journal of the American Chemical Society 114:2482-2494
28. Karlin KD, Nasir MS, Cohen BI, Cruse RW, Kaderli S, Zuberbuhler AD (1994) Journal of the American Chemical Society 116:1324-1336
29. Pidcock E, Obias HV, Zhang CX, Karlin KD, Solomon EI (1998) Journal of the American Chemical Society 120:7841-7847
30. Palavicini S, Granata A, Monzani E, Casella L (2005) Journal of the American Chemical Society 127:18031-18036
31. Mirica LM, Vance M, Rudd DJ, Hedman B, Hodgson KO, Solomon EI, Stack TDP (2005) Science 308:1890-1892
32. Mirica LM, Ottenwaelder X, Stack TDP (2004) Chemical Reviews 104:1013-1045
33. Que L, Tolman WB (2002) Angewandte Chemie-International Edition 41:1114-1137
34. Becke AD (1993) Journal of Chemical Physics 98:5648-5652
35. Lee CT, Yang WT, Parr RG (1988) Physical Review B 37:785-789
36. Schrödinger LLC (2003), Portland, OR
37. Hay PJ, Wadt WR (1985) Journal of Chemical Physics 82:299-310
38. Frisch MJ, Trucks GW, Schlegel HB, Scuseria GE, Robb MA, Cheeseman JR, Montgomery Jr. JA, Vreven T, Kudin KN, Burant JC, Millam JM, Iyengar SS, Tomasi J, Barone V, Mennucci B, Cossi M, Scalmani G, Rega N, Petersson GA, Nakatsuji H, Hada M, Ehara M, Toyota K, Fukuda R, Hasegawa J, Ishida M, Nakajima T, Honda Y, Kitao O, Nakai H, Klene M, Li X, Knox JE, Hratchian HP, Cross JB, Bakken V, Adamo C, Jaramillo J, Gomperts R, Stratmann RE, Yazyev O, Austin AJ, Cammi R, Pomelli C, Ochterski JW, Ayala PY, Morokuma K, Voth GA, Salvador P, Dannenberg JJ, Zakrzewski G, Dapprich S, Daniels AD, Strain MC, Farkas O, Malick DK, Rabuck AD, Raghavachari K, Foresman JB, Ortiz JV, Cui Q, Baboul AG, Clifford S, Cioslowski J, Stefanov BB, Liu G, Liashenko A, Piskorz P, Komaromi I, Martin RL, Fox DJ, Keith T, Al-Laham MA, Peng CY, Nanayakkara A, Challacombe M, Gill PMW, Johnson B, Chen W, Wong MW, Gonzalez C, Pople JA (2003). Gaussian, Inc., Pittsburgh, PA
39. Dunning TH (1989) Journal of Chemical Physics 90:1007-1023
40. Woon DE, Dunning TH (1994) Journal of Chemical Physics 100:2975-2988
41. Tannor DJ, Marten B, Murphy R, Friesner RA, Sitkoff D, Nicholls A, Ringnalda M, Goddard WA, Honig B (1994) Journal of the American Chemical Society 116:11875-11882
42. Marten B, Kim K, Cortis C, Friesner RA, Murphy RB, Ringnalda MN, Sitkoff D, Honig B (1996) Journal of Physical Chemistry 100:11775-11788
43. Curtiss LA, Raghavachari K, Redfern PC, Pople JA (2000) Journal of Chemical Physics 112:7374-7383
44. Siegbahn PEM, Blomberg MRA (1999) Annual Review of Physical Chemistry 50:221-249
45. Salomon O, Reiher M, Hess BA (2002) Journal of Chemical Physics 117:4729-4737
46. Reiher M, Salomon O, Hess BA (2001) Theoretical Chemistry Accounts 107:48-55
47. Cramer CJ, Tolman WB (2007) Accounts of Chemical Research 40:601-608
48. Lewin JL, Heppner DE, Cramer CJ (2007) Journal of Biological Inorganic Chemistry 12:1221-1234

49. Cramer CJ, Kinal A, Wloch M, Piecuch P, Gagliardi L (2006) Journal of Physical Chemistry A 110:11557-11568
50. Cramer CJ, Kinal A, Wloch M, Piecuch P, Gagliardi L (2007) Journal of Physical Chemistry A 111:4871-4871
51. Siegbahn PEM (2003) Journal of Biological Inorganic Chemistry 8:577-585
52. Cramer CJ, Wloch M, Piecuch P, Puzzarini C, Gagliardi L (2006) Journal of Physical Chemistry A 110:1991-2004
53. Malmqvist PA, Pierloot K, Shahi ARM, Cramer CJ, Gagliardi L (2008) The Journal of Chemical Physics 128:204109-204110
54. Gherman B, Cramer C (2008) Coordination Chemical Reviews ASAP, doi:10.1016/j.ccr.2007.11.018.
55. Mirica L (2005). PhD Thesis. Standford University. Available via the ProQuest database, UMI # 3162369
56. Mirica LM, Rudd DJ, Vance MA, Solomon EI, Hodgson KO, Hedman B, Stack TDP (2006) Journal of the American Chemical Society 128:2654-2665
57. Becke AD (1988) Physical Review A 38:3098-3100
58. Perdew JP, Chevary JA, Vosko SH, Jackson KA, Pederson MR, Singh DJ, Fiolhais C (1992) Physical Review B 46:6671-6687
59. Perdew JP, Burke K, Wang Y (1996) Physical Review B 54:16533-16539
60. Stephens PJ, Devlin FJ, Chabalowski CF, Frisch MJ (1994) Journal of Physical Chemistry 98:11623-11627
61. Vosko SH, Wilk L, Nusair M (1980) Canadian Journal of Physics 58:1200-1211
62. Hertwig RH, Koch W (1997) Chemical Physics Letters 268:345-351
63. Gherman BF, Tolman WB, Cramer CJ (2006) Journal of Computational Chemistry 27:1950-1961
64. Burke K, Ernzerhof M, Perdew JP (1997) Chemical Physics Letters 265:115-120
65. Becke AD (1996) Journal of Chemical Physics 104:1040-1046
66. Atkins P, De Paula J (2006) Physical Chemistry. Oxford University Press, Oxford
67. Mahadevan V, Henson MJ, Solomon EI, Stack TDP (2000) Journal of the American Chemical Society 122:10249-10250
68. Hatcher LQ, Vance MA, Sarjeant AAN, Solomon EI, Karlin KD (2006) Inorganic Chemistry 45:3004-3013
69. Itoh S, Taki M, Nakao H, Holland PL, Tolman WB, Que L, Fukuzumi S (2000) Angewandte Chemie-International Edition 39:398-400
70. Naka H, Kondo Y, Usui S, Hashimoto Y, Uchiyama M (2007) Advanced Synthesis & Catalysis 349:595-600
71. Himmelwright RS, Eickman NC, Lubien CD, Lerch K, Solomon EI (1980) Journal of the American Chemical Society 102:7339-7344
72. Winkler ME, Lerch K, Solomon EI (1981) Journal of the American Chemical Society 103:7001-7003